Theoretical and experimental study of hydrodynamics of metal target irradiated by ultrashort laser pulse

N.A. Inogamov*[a], S.I. Anisimov[a], Yu.V. Petrov[a], V.A. Khokhlov[a],
V.V.Zhakhovskii[b,c], K. Nishihara[c], M.B. Agranat[b], S.I. Ashitkov[b], P.S. Komarov[b]

[a]L.D. Landau Institute for Theoretical Physics, Chernogolovka, Russia
[b]Joint Institute of High Temperatures, Moscow, Russia
[c]Institute of Laser Engineering, Osaka University, Osaka, Japan

ABSTRACT

Theoretical consideration of the ablation of laser heated metal target based on two-temperature hydrodynamic calculation is performed for aluminum and gold targets. Concurrent with the hydrodynamic calculation the molecular dynamics simulation of the ablation was carried out in the case of aluminum. The initial state of matter for the molecular dynamics is taken as a final state of hydrodynamic calculation. Molecular dynamics simulation is extended to cover late stages of the evolution of two-phase foam placed between the crater and spalled cupola. Theoretical results are in a good agreement with the experimental data obtained by the microinterferometer diagnostics of the femtosecond laser ablation both for aluminum and gold.

Keywords: femtosecond laser, ablation, two-temperature hydrodynamics, molecular dynamics

1. INTRODUCTION

To study the ablation of condensed matter targets exposed to the femtosecond laser irradiation molecular dynamics is the effective tool because it naturally includes phase transitions which occur in the expanding target[1-8]. When using the molecular dynamics simulation we are dealing with the matter atoms as the nonstructural objects. Even if sufficiently complex interatomic interaction potentials, such as many body potentials of metals,[9,10] including the effect of ion interaction through the conduction electrons, are used, the molecular dynamics describes the motion of atomic nuclei only. So even in this case the paricles used in the molecular dynamics simulation have no internal structure. That is why the molecular dynamics in this form has to be one-temperature. But at the earlest stage of the interaction of laser radiation with a metal the temperatures of conduction electrons and ions are significantly different because of the large difference in electron and ion mass.[11] Due to this large mass difference the energy is slowly transmitted from electrons to ions and the state of metal in this structure is two-component (electrons and ions) and two-temperature. At this stage of ablation the two-temperature hydrodynamics approach[12] seems to be the most adequate to describe electron and ion motion to give the initial state for one-temperature molecular dynamics simulation at later instants. Molecular dynamics simulation allows considering the onset of ablation process and the formation of a condensed matter spalled cupola filled with a two-phase mixture. In the late stages molecular dynamics shows the significant growth of vapor bubbles within the two-phase mixture and formation of nano-relief on a cupola and a crater in the bulk target and separation of spalled layer from a target. Both theoretical and experimental study of optical diagnostics of the spalled cupola is carried out for aluminum and gold. Experimental investigation is based on the pump-probe microinterferometer scheme, while theoretical approach lies in the calculation of reflection coefficient and phase shift when the probe beam reflects from the multi-layer matter (spalled cupola, two-phase mixture, and crater bottom).

*nailinogamov@googlemail.com

High-Power Laser Ablation VII, edited by Claude R. Phipps
Proc. of SPIE Vol. 7005, 70052F, (2008) · 0277-786X/08/$18 · doi: 10.1117/12.782598

2. TWO-TEMPERATURE HYDRODYNAMICAL STAGE

When a femtosecond laser pulse impinges on a metal target, the laser energy is absorbed by electrons in a conduction band leading to the significant excess of the electron temperature over practically cold ion lattice. The thickness of the absorption layer is of the order of skin depth and comprises about ten nm for simple metals. Heat energy obtained from the laser by electrons is transmitted into the bulk target by the electron heat conductivity. At the same time the energy is transferred from electrons to ions to equalize electron and ion temperatures. This electron-ion energy exchange rate is inversely proportional to the ion mass, so that the time of the equalization of electron and ion temperatures τ_{ie} is proportional to the ion mass *M*. Taking into account that the sound speed c_s is inversely proportion to the square root of *M*, the linear expansion of a matter during the time interval τ_{ie} can be estimated as proportional to the square root of *M*. So for light metals as aluminum, up to the instant when electron and ion temperatures became equal the linear shift of matter and a volume change are very small. This first stage is therefore finished by the heating of some finite layer of a metal (of hundred nm thickness) with equal electron and ion temperatures and essentially unchanged density. The state of matter at the end of this stage can be further used as the initial state for molecular dynamics simulation for later expansion of such heated layer of a metal.

In studies of the ablation of metals on exposure to femtoseciond laser irradiation, the linear shift of the expanding matter in the direction of laser beam in a time under considaration does not exceed μm scale, while the cross diameter of a laser beam can achieve 80 μm. Thus the hydrodynamic motion of a matter can be considered as one-dimensional. When electrons and ions have different temperatures, the hydrodynamic equations describing their motion must be two-temperature. Because of the presence of boundaries between different phases of a matter the Lagrangian scheme of hydrodynamics looks preferable. The two-temperature Lagrange equations together with the absorption of laser radiation and the energy exchange between electrons and ions can be written as follow

$$
\begin{aligned}
\rho^0 \frac{\partial v}{\partial t} &= -\frac{\partial p}{\partial x^0}, \quad p = p_i + p_e \\
\frac{\partial x}{\partial t} &= v, \quad \rho = \frac{\rho^0}{\frac{\partial x}{\partial x^0}}, \\
\rho^0 \frac{\partial E_e(\rho, T_e)}{\partial t} - \frac{\partial}{\partial x^0}\left(\frac{\rho \kappa_e(\rho, T_e, T_i)}{\rho^0} \frac{\partial T_e}{\partial x^0} \right) &= -p_e \frac{\partial v}{\partial x^0} + \lambda (T_i - T_e) + Q, \qquad (1) \\
\rho^0 \frac{\partial E_i(\rho, T_i)}{\partial t} - \frac{\partial}{\partial x^0}\left(\frac{\rho \kappa_i(\rho, T_i)}{\rho^0} \frac{\partial T_e}{\partial x^0} \right) &= -p_i \frac{\partial v}{\partial x^0} - \lambda (T_i - T_e), \\
p_e = p_e(\rho, T_e), \quad p_i &= p_i(\rho, T_i)
\end{aligned}
$$

Here ρ is a matter density, ρ^0 is the initial density, when the Lagrange particles with coordinates $x = x(x^0, t)$ occupy their initial positions $x^0 = x(t = 0)$; v is a matter velocity; T_e, p_e, E_e and T_i, p_i, E_i are, correspondently, electron and ion temperature, pressure and internal energy. p is total pressure (electron and ion), κ_e and κ_i are the electron and ion heat conductivities. In practice we do not take into account ion heat conductivity as it is negligibly small. λ is the electron-ion energy exchange rate (the energy transferred from electrons to ions per unit time and unit

volume; Q is the energy absorbed by electrons from the laser radiation per unit time, per unit volume. The temporal dependence of Q can be approximately presented by the Gaussian dependence $Q(t) = Q_0 \exp\left(-t^2/\tau^2\right)$ with the maximum laser intensity at the instant $t = 0$.

The result of solving equations (1) to obtain a state of an aluminum bulk target at instant $t = 0$ is shown in Fig.1 for the laser pulse with fluence at the center of beam $F_c = 70$ mJ/cm^2.

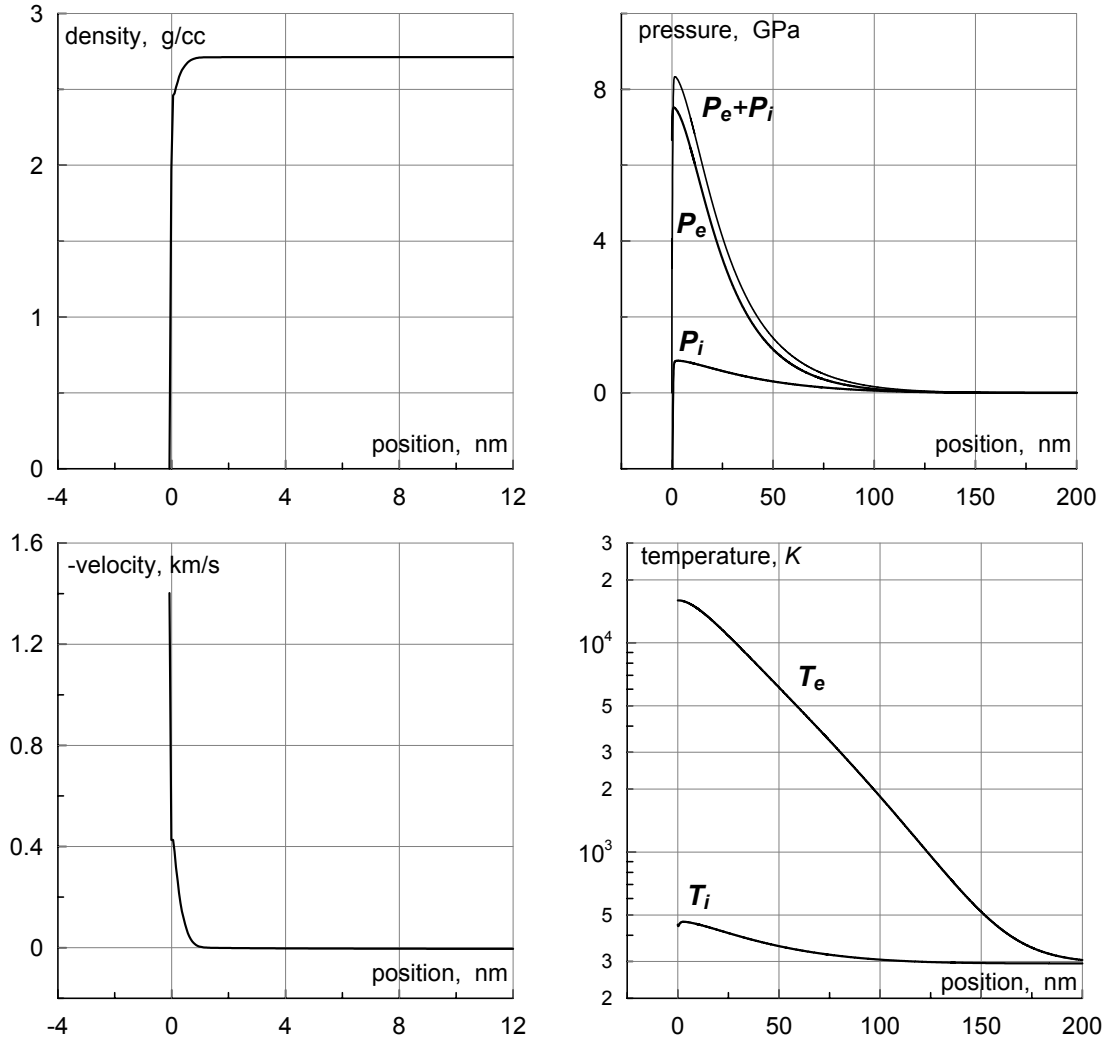

Fig. 1. Parameters of aluminum bulk target at time instant $t = 0$, when the laser pulse has its maximum intensity. Right figures occupy 10 times larger space interval than left figures. At this instant the target velocity and shift of its surface are negligibly small, but the thickness of a target layer heated by the electron heat conductivity and energy exchange between electrons and ions essentially exceeds the depth of penetaration of laser radiation into the target. There is a large difference between electron and ion temperatures.

As it can be seen from Fig.1 at the instant of maximum laser intensity the displacement of a target surface is practically absent, so the target density does not change. Difference between electron and ion temperatures is very large. The state of target at the instant $t = 3\tau$ is shown in Fig.2, when the action of a laser is really completed.

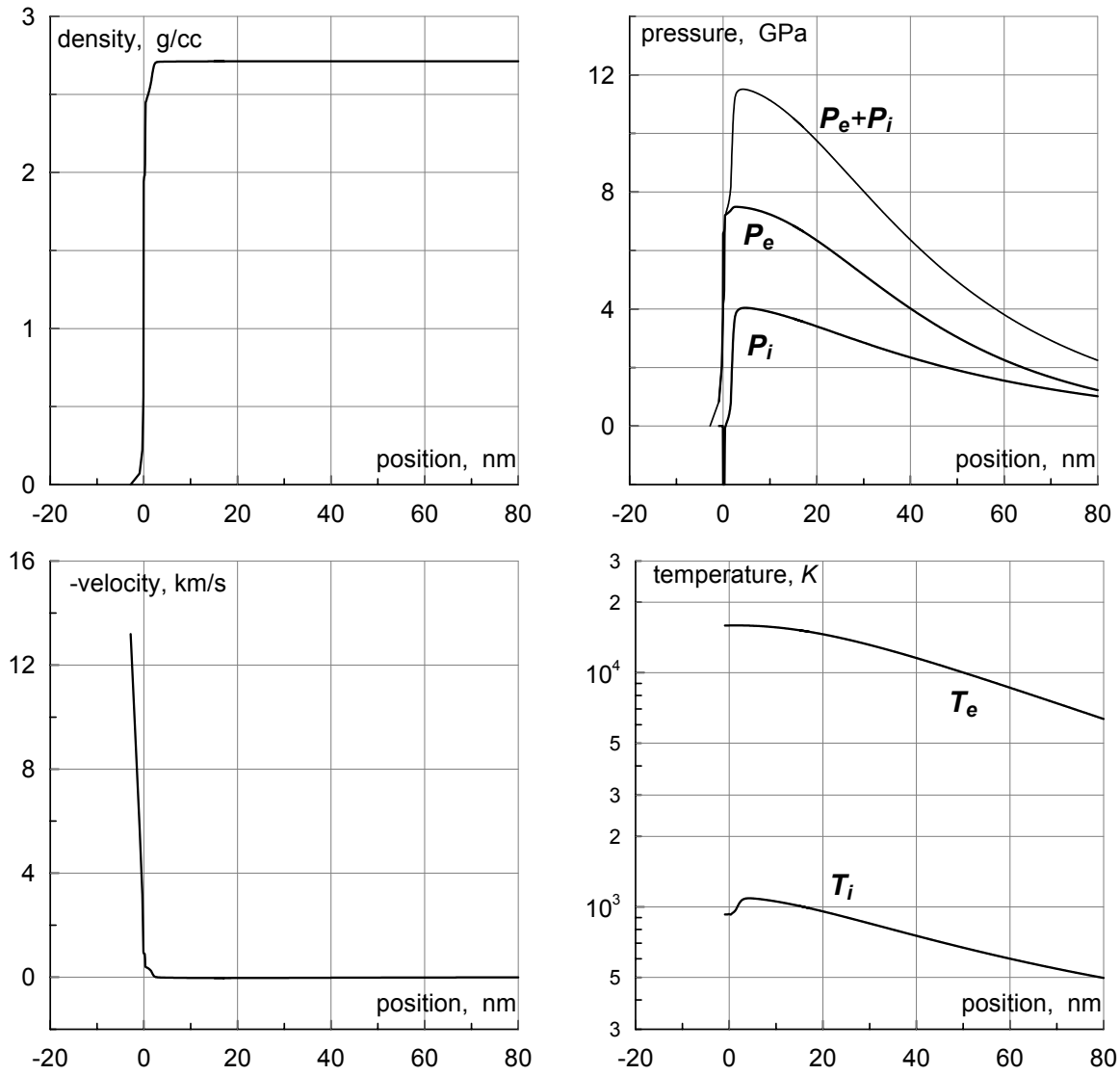

Fig. 2. Parameters characterizing the state of an aluminum target at the instant $t = 3\tau$ (0.3 ps), when the action of a laser pulse is completed. The ion temperature is smaller than the electron temperature and the matter motion is faintly visible as before.

At the instant corresponding to the cut off of the laser pulse the target matter does not essentially moves, so that it has unchanged density. Difference between electron and ion temperatures becomes smaller but is still large enough if one takes into account the logarithmic temperature scale. As time passes the electron and ion temperatures become closer to each other and the matter motion becomes more visible. The instant when electron and ion temperatures become substantially equal corresponds to 4 ps measured from the instant of maximum laser intensity for aluminum target. The values characterizing the state of a target at this time instant are shown in Fig. 3. Equal electron and ion temperature spatial profiles at this instant can be well enough approximated by the Gaussian-type curve. Density change is sufficiently small with respect to the undisturbed target so the equalization of electron and ion temperatures occurs in fact in the isochoric regime. This isochorically heated target with Gaussian spatial distribution of a temperature inside the bulk sample can be thus used as the initial state for the further use for molecular dynamics simulation. Molecular dynamics simulation is preferable at the stage of expansion of heated target because this expansion is accompanied by phase transitions in a target matter, naturally described by molecular dynamics approach.

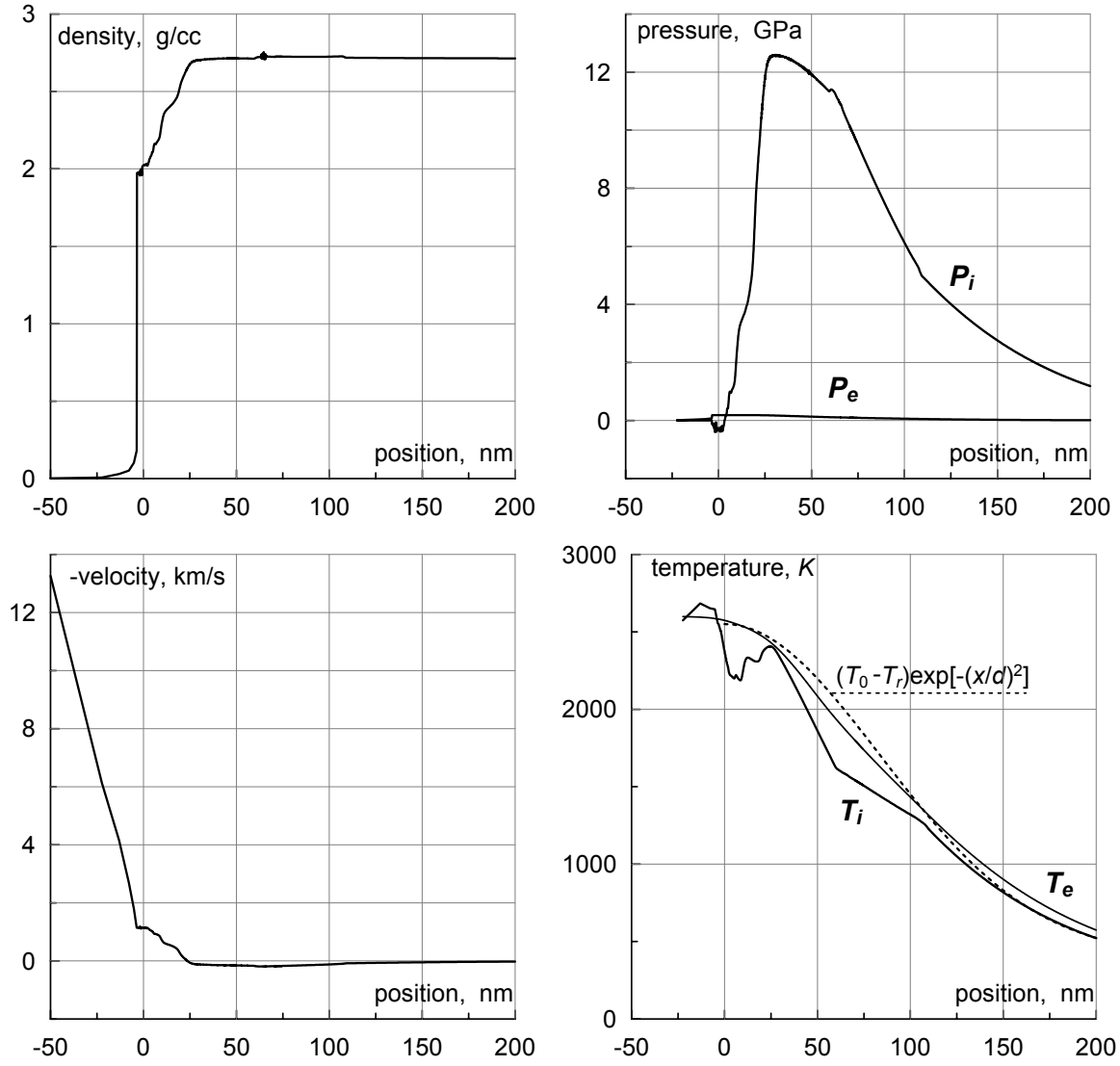

Fig. 3. Values characterizing the state of aluminum target at the instant when electron and ion temperatures become equal.

3. MOLECULAR DYNAMICS SIMULATION OF EXPANSION OF HEATED TARGET

Because of the mentioned above essential exceed of the transversal size of laser beam over the longitudinal displacement of the expanding target matter in the direction perpendicular to the target surface it is possible to consider in molecular dynamics simulation only this longitudinal (quasi one-dimensional) expansion of a heated target. Taking into account nearly Gaussian form of radial distribution $F(r)$ of fluence across the laser beam $F(r) = F_c \exp(-r^2 / R_L^2)$ with a maximum fluence F_c in the center of beam of radius R_L, one obtaines similar distribution of the temperature over a heated target. Different initial temperatures across the laser heated spot on the target lead to different shift of matter. Radial pattern of transformation of target matter over the laser heated spot on a target is shown in Fig. 4 at three instants.

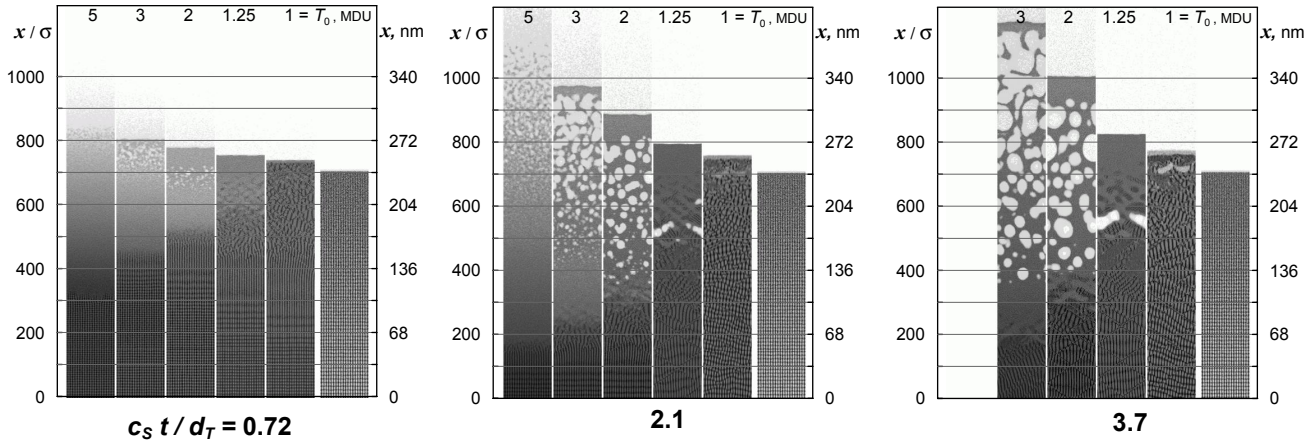

Fig. 4. Density maps obtained in set of MD simulations illustrate the transformation of target material along the radius of laser hot spot at three dimensionless times. The center of spot is located in the left side of each figure. Right axes in nm units correspond to the Lennard-Jones potential for Argon with σ = 0.3405 nm.

Molecular dynamics simulation in Fig. 4 is made by using of the Lennard-Jones interaction between atoms. d_T is the depth of heated part of target and c_s is the sound speed. The outstanding part of the ablation pattern is a runaway layer at vertical columns, reducing in thickness when approaching the center of spot. Assembled together these runaway layers form a runaway condensed matter cupola, drawn in Fig. 5.

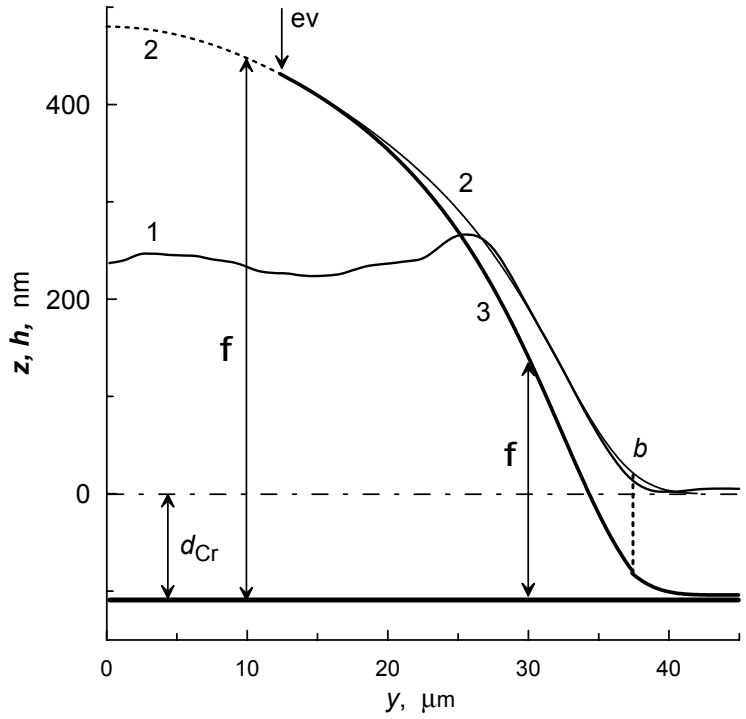

Fig. 5. The form of spalled cupola consisted of condensed material. Side view of a target. d_{Cr} is the depth of crater in a target. The area between the spalled cupola and the crater is filled by two-phase mixture of condensed material and its vapor.

In Fig. 5 the spalled cupola is formed by the condensed matter placed between the lines 2 and 3. Its thickness drops when the radial coordinate y approaches the center of a spot and becomes zero at the position marked by the arrow "ev". It results in a hole within a cupola at its center. The region between the cupola and a bottom of a crater in the target is occupied by the mixture of a condensed matter and its vapor. The formation of this two-phase mixture is clearly visible in the left column of shots in Fig. 4. When ablation starts from liquid surface target (for example in metals the fluence threshold for the onset of ablation always exceeds the melting threshold), at significant expansion of matter two-phase region consists of vapor bubbles separated by thin liquid membranes. Expansion of matter causes an increase of a surface energy connected with the membranes. It results in the essential restore of tensile pressure even at significant shift of a runaway cupola and additional prolonged deceleration of a cupola. This large shift of the condensed matter cupola due to the deceleration by the bubble-membrane mixture to a great extent exceeds the simple heat expansion length. It is true to say that the bubble-membrane mixture has ultrahigh stretchibility plasticity. As the matter expansion increases the size of bubbles increases too. At the last stage of expansion their diameters become comparable to the laser heated depth d_T in the target. Initially flat target surface is gradually deformed because of the growth of bubbles under the runaway layer. It gives rise to a ribbing of the surface (Fig. 6).

At time interval $t \sim 1$ ns essential cooling of laser heated target layer takes palace due to the the heat conduction into the internal region of a target. It leads to the crystallization of a liquid bottom of crater with a well visible nanostructure.

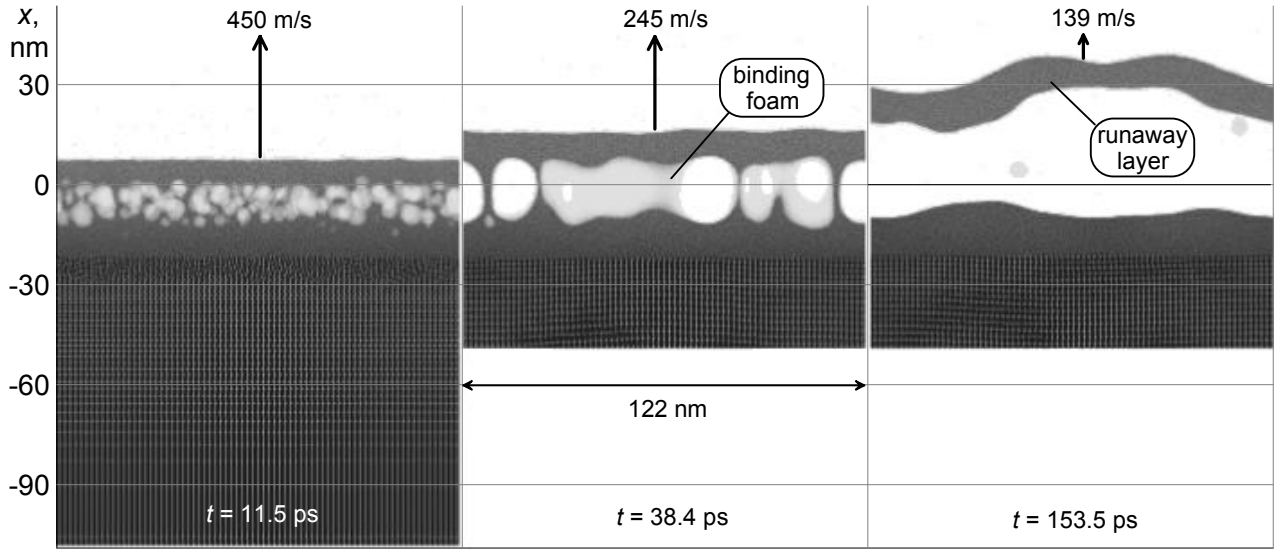

Fig. 6. Gradual nanomorphological transformation on the external surface of spalled (runaway) layer moving from aluminum target simulated by MD using Mishin et.al. potential[10]. This transformation is caused by evolution of the ansemble of cavitational bubbles. Nucleation of bubbles shown in the left shot, their growth in the middle shot. The right shot illustrates the separation of runaway layer from the target.

4. EXPERIMENTAL MICROINTERFEROMETER INVESTIGATION OF THE ABLATION OF METALS SUBJECTED TO FEMTOSECOND LASER PULSE

A good tool to investigate very small (up to nm) displacement of the laser irradiated target surface is the pump-probe laser scheme[13-15] with the use of Michelson-type microinterferometer measurements.[16-18] The experiments were performed using high power chromium-doped forsterite laser with pulse duration of 100 fs.[18] Measuring the shift of interference strips it is possible to connect it with the dispalacement of a target matter. The external side of the runaway cupola in Fig. 5 is constructed from the direct experimental measurements of the phase shift of reflected from the gold target probe laser beam. When the thickness of a cupola is thick enough, the phase shift follows the external boundary of

a cupola. At small values of a cupola thickness the phase shift line 1 essentially deviates from the cupola boundary, so that the phase shift is saturated. This deviation takes place when the reflection from the crater bottom exceeds the reflection from the runaway cupola. It happens at the significant decrease of cupola thickness from the value $h \approx 110$ nm for aluminum target at the ablation threshold (crater depth, b mark in Fig. 5) to the value $h \approx 20$ nm. The saturation of the phase shift in the microinterferometer experiments begins at smaller fluence values than evaporation threshold. That is why the hole, visible in microinterferometer, is wider than the real hole in a runaway condensed matter cupola. Experimental interferogram with a deviation of interference strips and a hole in the center is presented at the middle shot in Fig. 7.

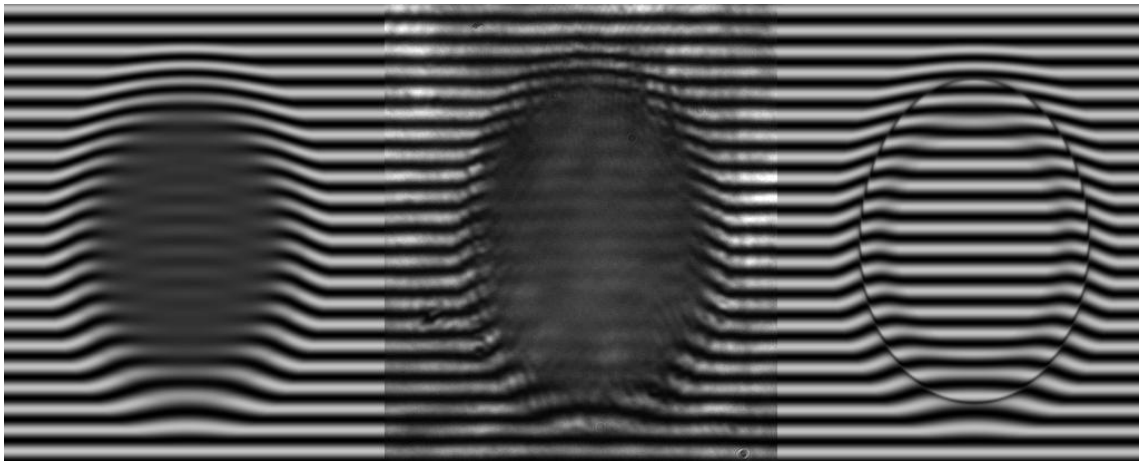

Fig. 7. Comparison of the experimental and calculated interferograms for gold target.

Left and right shots in Fig. 7 show theoretically calculated light intensity obtained as a result of interference of reflected from the target surface probe beam and reference beam. Reference beam propagates at a small angle to the reflected from the target probe beam. The geometry of a cupola is taken from Fig. 5 with the complex refraction index both for crater and cupola matter to be $n_{cr} = n_{cup} = 0.25 + 3.15i$ (data for solid gold refraction index at light wave length $\lambda = 620$ nm from[19]). At the right shot of Fig. 7 the complex refraction index in the two-phase mixture between the cupola and a crater was chosen simply as $n_{mix} = 1$, whereas at the left shot small light absorption in this region was taken into account ($n_{mix} = 1 + 0.2i$). With allowance for small light absorption within the two-phase foam the interference pattern becomes very close to that one experimentally detected. It displays the same deviation of interference strips and the appearance of a hole in the center of a pattern.

In Fig. 8 we compare the results obtained by the use of our two-stage calculation (two-temperature hydrodynamics and molecular dynamics simulation) with the experimental data near the ablation threshold. Experimental values of the reflection coefficient were used to obtain the absorbed fluence value. Squares in Fig. 8 mark the experimental values of the target surface displacement when the fluence doesn't exceed the ablation threshold to give the residual deformation. Corresponding theoretical curve (for initial surface temperature T_0 = 2590 K) is in a good agreement with experimental values. Cross marks in Fig. 8. correspond to the experimentally observed shift of target surface at the fluence exceeding the ablation threshold. Theoretical curve at the initial sirface temperature T_0 = 3 kK in this case is close to experimental one.

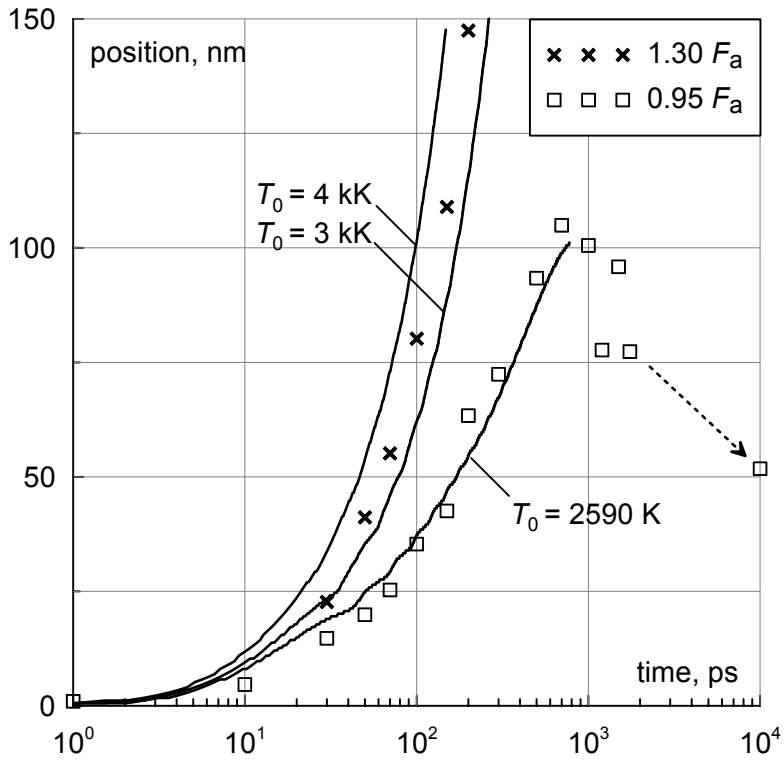

Fig. 8. Comparison of the theoretically calculated and experimentally measured shift of the target surface below (initial surface temperature $T_0 = 2590$ K) and above ($T_0 = 3$ kK and 4 kK) the ablation threshold $F_a = 0.74$ J/cm^2.

5. CONCLUSIONS

We presented investigation of thermomechanical and optical properties of matter when ablation takes place under the action of femtosecond laser irradiation onto metals. The molecular dynamics simulation with the use of many body interaction potentials together with the previously done two-temperature hydrodynamics at the early stage gives results which show the remarkable accord with the experimental data obtained by interferometric diagnostics of the ablation of metals. Being extended to the late stages of expansion of two-phase mixture between the spalled condensed matter cupola and crater, the molecular dynamics simulation displays the nanostructural deformation of the cupola and crater bottom.

ACKNOWLEDGEMENT

We are grateful to the Cybermedia Center at Osaka University for organization of MD simulations. This work is supported by the Grant RFBR 07-02-00764.

REFERENCES

[1] Zhigilei, L. V., Garrison, B. J., "Microscopic mechanizm of laser ablation of organic solids in the thermal and stress confinement irradiation regimes," Journ. Appl. Phys., 88 (3), 1281-1298 (2000).

[2] Perez, D., Lewes, L. J., "Ablation of solids under femtosecond laser pulses," Phys. Rev. Lett., 89 (25), 255504 (2002).

[3] Ivanov, D. S., Zhigilei, L. V., "The effect of pressure relaxation on the mechanisms of short pulse laser melting," Phys. Rev. Lett. 91, 105701 (2003).
[4] Anisimov, S. I., Zhakhovskii, V. V., Inogamov, N. A., Nishihara, K., Oparin, A. M., Petrov, Yu. V., "The breakup of a solid film as a result of the action of ultrashort laser pulse," JETP Lett., 77, 606 (2003).
[5] Leveugle, E., Ivanov, D. S., Zhigilei, L. V., "Photomechanical spallation of molecular and metal targets: molecular dynamics study," Appl. Phys. A 79, 1643 (2004).
[6] Anisimov, S. I., Zhakhovskii, V. V., Inogamov, N. A., Nishihara, K., Petrov, Yu. V., Khokhlov, V. A., "The expansion of matter and a crater formation under the action of ultrashort laser pulse," JETP, 103, 183 (2006).
[7] Upadhyay, A. K., Urbassek, H. M., "Response of ultrathin metal films to ultrafast laser irradiation: A comparative molecular-dynamics study", J. Phys. Conf. Ser. 59, 68-74 (2007)
[8] Bazhirov, T. T., Norman, G. E., Stegailov, V. V., "Cavitation in liquid metals under negative pressures. Molecular dynamics modeling and simulation", J. Phys.: Condens. Matter, 20 (11), 114113 (2008).
[9] Ercolessi, F., Adams, J. B., "Interatomic potentials from first-principles calculations: the Force-Matching method", Europhys. Lett., 26, 583 (1994).
[10] Mishin, Y., Farkas, D., Mehl, M. J., Papaconstantopoulos, D. A., "Interatomic Potentials for Monatomic Metals from Experimental Data and ab initio Calculations", Phys. Rev., B 59 (5), 3393–3407 (1999).
[11] Anisimov, S. I., Kapeliovich, B. L., Perl'man T. L., "Electron emission from metal surfaces exposed to ultrashort laser pulses", Sov. Phys. JETP, 39 (2), 375-377 (1974).
[12] Inogamov, N. A., Zhakhovskii, V. V., Petrov, Yu. V., Khokhlov, V. A., Ashitkov, S. I., Anisimov, S. I., Agranat, M. B., Nishihara, K., "Hydrodynamics of interaction of ultrashort laser pilse with a matter: Comparison of calculations with the experiment", Physics of the extermal states of matter, Chernogolovka, 172-174 (2008).
[13] Sokolowski-Tinten, K., Bialkovski, J., Cavalleri, A., von der Linde, D., "Observation of a transient insulating phase of metals and semiconductors during short-pulse laser ablation", Appl. Surf. Sci., 127-129, 755-760 (1998).
[14] Von der Linde , D., Sokolovski-Tinten, K., "The physical mechanisms of short-pulse laser ablation", Appl. Surf. Sci., 154-155, 1-10 (2000).
[15] Rethfeld, B., Temnov, V. V., Sokolowski-Tinten, K., Tsu, P., von der Linde, D., Anisimov, S. I., Ashitkov, S. I., Agranat, M. B., "Superfast thermal melting of solids under the action of femtosecond laser pulses," Journ. of Opt. Tech., 71 (6), 348-352 (2004).
[16] Temnov, V. V., Sokolowski-Tinten, K., Zhou, P., von der Linde, D., "Femtosecond time-resolved interferometric microscopy," Appl. Phys., A 78, 483-489 (2004).
[17] Widmann, K., . Guethlein, G., Foord, M. E., Cauble, R. C., Patterson, F. G., Price, D. F., Rogers, F. J., Springer, P. T., Stewart, R. E., Ng, A., Ao, T., Forsman, A. "Interferometric investigation of femtosecond laser-heated expanded states", Phys. of Plasmas, 8, 3869-3872, (2001).
[18] Agranat, M. B., Andreev, N. E., Ashitkov, S. I., Veisman, M. E., Levashov,P. R., Ovchinnikov, A. V., Sitnikov, D. S., Fortov, V. E., Khishchenko K. V. "Determination of the transport and optical properties of a nonideal solid plasma produced by femtosecond laser pulses", JETP Lett., 85, 271–276, (2007).
[19] Palik, E. D., (ed.), [Handbook of Optical Constants of Solids III. Volime 1], Academic Press, New York (1998).